(vi) Oxygen minimum zones and biogeochemical cycling in the EBCS: Oxygen minimum zones (OMZ) are regions of the global ocean, located at intermediate depths (50–1000 m), with dissolved oxygen concentrations less than 0.5 mL L^{-1} (i.e. about 7.5% saturation, <22 μM) due to reduced ventilation and the high respiration rates of the settling organic matter produced in the surface waters (Levin 2003). Of the four EBCS, three (Benguela, California, Humboldt) have an important OMZ (Kamykowski and Zentara 1990). Recent and comprehensive reviews of the OMZ can be found in Levin (2003), Karstensen et al. (2008), and Paulmier and Ruiz-Pino (2008). Oxygen minimum zones play a crucial role in the ecology and biogeochemistry of the EBCS. They constitute an important physical barrier for aerobic respiration, making oxygen levels a critical factor for the distribution and survival of the pelagic biota (e.g. Boyd et al. 1980, Morales et al. 1996, González and Quiñones 2002, Chan et al. 2008), especially in those regions of the EBCS with an intense and shallow OMZ.

The co-existence of oxic–suboxic gradients in the OMZ involves rather complex biogeochemical processes such as strong organic matter remineralization, nitrate removal, and nitrite release (Paulmier and Ruiz-Pino 2008). Furthermore, OMZ are important sources of the greenhouse gases carbon dioxide (CO_2) and nitrous oxide (N_2O) (Ward et al. 1989, Cornejo et al. 2006, Farías et al. 2007). On the other hand, accumulating evidence indicates that the microbial communities inhabiting the OMZ of the EBCS are very active metabolically (e.g. Kyupers et al. 2005, Molina et al. 2005, González et al. 2007, Levipan et al. 2007) and present high diversity (e.g. Molina et al. 2007, Woebken et al. 2008, Quiñones et al. 2008, Stevens and Ulloa 2008). Despite the importance of the OMZ in the global nitrogen cycle, little is known about the structure and functioning of its microbial communities. The physical dynamics and the mechanisms by which the OMZ are maintained in the Benguela, California, and Humboldt systems are also poorly understood.

The high spatial and temporal variabilities as well as the open nature of the EBCS boundaries are important limitations for the carbon and nutrient budgets estimated therein (Sects. 2.2, 2.3, 2.4, 2.5, and 2.6). An improved modeling approach (e.g. Baird et al. 2007) is an important step toward achieving better carbon and nutrient estimates. However, what is really necessary in order to confront some of the issues listed above is a more thorough integration of population–community and process–functional approaches (sensu O'Neill et al. 1986).

2.2 The Northern and Central California Coastal Upwelling System

J. Timothy Pennington,
Gernot E. Friederich, Carmen G. Castro,
Curt A. Collins, Wiley W. Evans
and Francisco P. Chavez

2.2.1 Introduction

2.2.1.1 The Carbon Cycle: CO_2, the Greenhouse Effect, and the Biological Pump

Over the past 150 years, carbon dioxide (CO_2) has accumulated in the atmosphere and the partial pressure of CO_2 (pCO_2) has increased from approximately 280 to 370 ppm primarily due to the burning of fossil fuels, currently at a rate of about 6.5 gt carbon yr^{-1} (see overview in Miller, 2004). Because CO_2 absorbs infrared radiation, increased atmospheric CO_2 decreases radiative heat loss to space – the 'Greenhouse effect' – leading to the prediction that human activity is warming the earth's climate. While data confirm that climate is warming, many associated rates, patterns, and interactions remain poorly understood. These uncertainties have prompted considerable study of carbon cycles, of which this article and book are part. AQ2

The atmospheric accumulation of CO_2 is moderated by the existence of CO_2 sinks such as the oceans. The increase of atmospheric CO_2 has produced disequilibrium between the surface ocean and the atmosphere, which on average forces CO_2 to diffuse into the ocean (Bates, 2001; Bates et al., 2001; Sabine et al., 2004). About 1.7 gt carbon yr^{-1} or 30%

J.T. Pennington (✉)
Monterey Bay Aquarium Research Institute, Moss Landing, CA 95039, USA
e-mail: peti@mbari.org

of the annual atmospheric CO_2 input is estimated to dissolve in the surface ocean (see Miller, 2004; Sabine et al., 2004). Biological processes play a pivotal role in determining sea surface pCO_2 (see Hayward, 1991). When phytoplankton convert CO_2 into organic molecules and their cellular constituents via photosynthesis (carbon 'fixation'), near-surface pCO_2 levels are reduced and the gradient between atmosphere and ocean is, on average, increased. When phytoplankton are eaten or die, a portion of their fixed carbon sinks, thus removing carbon from the lighted euphotic zone. These two processes, carbon fixation by photosynthesis and sinking, are termed the 'biological pump' and in combination they maintain low near-surface pCO_2, promoting carbon transfer from the atmosphere into the oceans by diffusion. Beneath the euphotic zone, organism respiration converts phytoplankton organic carbon back into CO_2 and other inorganic carbon species ('remineralization'), and this CO_2 is isolated from the atmosphere for hundreds to thousands of years (Falkowski et al., 1998). The biological pump is also regulated by iron, nitrate, and other factors, but in its absence CO_2 concentration in the atmosphere would be substantially higher (Miller, 2004; Sabine et al., 2004).

There are strong spatial and temporal variations in ocean/atmosphere CO_2 interactions. Ocean temperature change is important due to its effect on gas solubility. In regions with equatorward flowing and thus warming surface currents, gas solubility decreases and CO_2 is in general vented to the atmosphere; the converse occurs in regions with poleward-flowing currents. Biology interacts with physics to complicate matters. In the equatorial upwelling regions, subsurface water supersaturated in CO_2 is drawn to the surface, the biological pump operates slowly due to iron limitation, and about 1 Gt carbon is vented into the atmosphere annually (Chavez et al., 1999). Climactic variations, such as El Niño and El Viejo (Chavez et al., 2003), further alter these processes. For many parts of the oceans such as the coastal margins, CO_2 fluxes into and from the ocean have not been measured at all (see Liu et al., 2000), and the cycles and rates that control the biological pump have not been examined or synthesized. These processes are important, especially as feedbacks to climate change phenomena. Do coastal upwelling systems contribute to atmospheric CO_2 as does equatorial upwelling? Studies to examine the contributing elements of carbon cycles in such locations are badly needed. One such location is the coastal upwelling region of the northeast Pacific.

2.2.1.2 The Northeast Pacific Eastern Boundary and Coastal Upwelling System

The Pacific Ocean off western North America is a classic eastern boundary current region (Fig. 2.2.1; see Barber and Smith, 1981; Thurman and Trujillo, 1999). In this system near-surface flow of the gyral circulation can be divided into three regions. Offshore, in the central Pacific beyond about 1300 km from North America, warm and salty North Pacific Central Gyre (NPCG) waters form a southward-flowing layer about 250 m deep (reviewed by Karl and Lucas, 1996). Second, between the NPCG and 150–200 km west of North America, the California Current (CC) also flows southward at 0.6–1.2 km h^{-1} (U.S. Hydrographic Office, 1947) as a 1200 km broad and 250 m deep surface current (Reid et al., 1958). CC isolines (thermocline, halocline, nutricline; Fig. 2.2.2A–F) shoal toward the east due to a basin-scale geostrophic adjustment termed 'pycnocline tilting', caused by the interaction of the flow with Coriolis (Chelton et al., 1982). Maximum velocity occurs near the CC's eastern margin, on average only 150–200 km offshore (Fig. 2.2.3), and this 'CC jet' or core transports the CC's lowest salinity water (see Fig. 2.2.2C, D; Lynn and Simpson, 1987; Strub and James, 2000; Collins et al., 2003). Spring and summer maxima in CC jet velocity are associated with seasonal maxima in CC pycnocline tilting (Collins et al., 2003). Third, inshore of the CC jet, the CC interacts with the North American continent in a region we call the coastal upwelling system (CUS), where coastal currents and mesoscale phenomena dominate (Barber and Smith, 1981; Collins et al., 2003). In spring and summer, seasonal northwesterly winds drive a coastal upwelling circulation in the CUS characterized by equatorward flow of near-surface coastal upwelling jets with associated eddies and fronts that extend offshore to the CC jet (Fig. 2.2.3). During upwelling, isolines in the CUS shoal and inshore near-surface waters become colder and saltier (Fig. 2.2.2A–D; reviewed by Pennington and Chavez, 2000; Chavez et al., 2002, 2003) – distinct from CC jet waters offshore (Fig. 2.2.2A–D; Collins et al., 2003). This wind-driven equatorward circulation overlies the poleward-flowing California

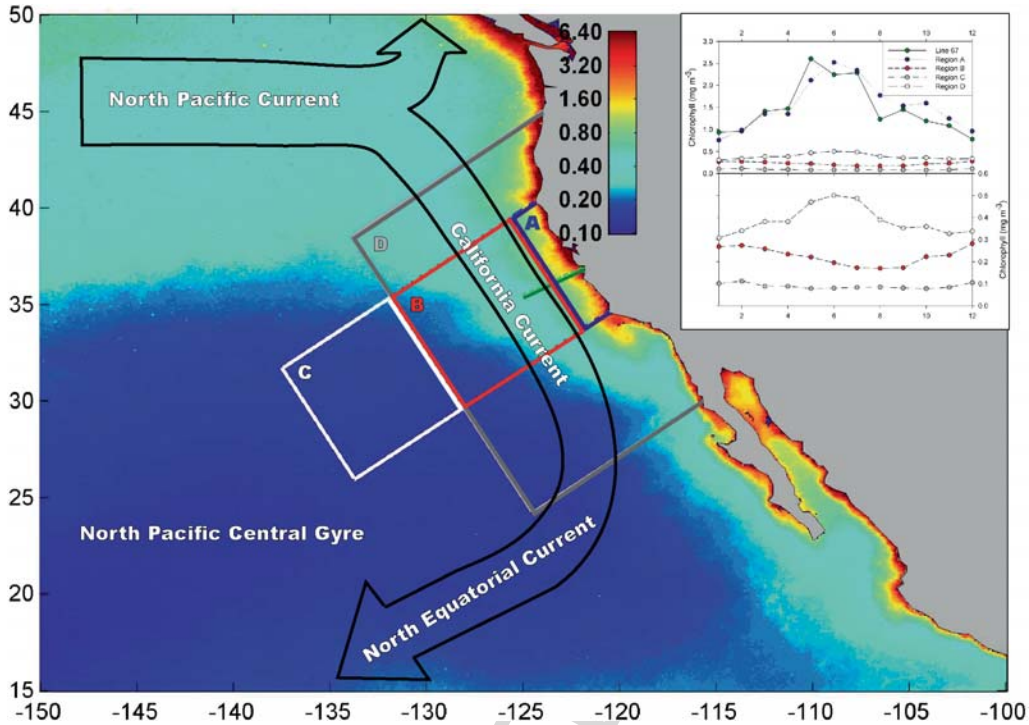

Fig. 2.2.1 NE Pacific composite SeaWIFS surface chlorophyll image, with schematic currents overlain. The carbon budget is assembled for the CUS (Region A), which is defined as a 60 m deep Ekman layer reaching from Cape Mendocino to Point Conception and 170 km offshore along CalCOFI Line 67 (L67; *green dots*). Monterey Bay is at the NE terminus of L67. The Behrenfeld and Falkowski (1997) net primary production model (Table 2.2.3) was run for the CUS (Region A), the central CC (Region B), a portion of the NPCG (Region C), and the larger CC (Region D). The inset compares monthly surface chlorophyll values for the regions of Fig. 2.2.1 and L67. L67 and the CUS (Region A) are very similar (*upper panel*), the larger CC including the CUS (Region D) is much lower but still exhibits a spring/summer maximum (*lower panel*), while the offshore CC (Region B) and the NPCG (Region C) exclude the CUS and lack a spring/summer chlorophyll maximum (*lower panel*)

Undercurrent, which has maximum velocity near 100 m but reaches to at least 1000 m (Collins et al., 2000). In winter, the northwesterly winds weaken or are replaced by southerly storm winds. Under these conditions the California Undercurrent surfaces (Sverdrup et al., 1942; Reid and Schwartzlose, 1962), where it is called the Inshore Countercurrent or Davidson Current which flows northward 0–100 km offshore (Collins et al., 2000). The CC and CUS with its California Undercurrent, Inshore Countercurrent and coastal upwelling circulation are together termed the California Current System (CCS; Collins et al., 2003).

Biologically, the CUS, CC, and NPCG progress from eutrophic coastal to oligotrophic central waters (Barber and Smith, 1981). During the spring and summer in the CUS, wind-driven upwelling draws the nutricline into the euphotic zone (Fig. 2.2.2E–F) and the enhanced nutrient flux supports prolific phytoplankton growth (Fig. 2.2.2G–J), in particular of large cells such as diatoms (Pennington and Chavez, 2000; see Chavez et al., 2002, for El Niño perturbations). This upwelling season primary production in turn supports stocks of zooplankton (Hopcroft et al., 2002; Marinovic et al., 2002), fishes (Chavez et al., 2003), and cetaceans (Benson et al., 2002). The CC jet may act as a barrier which separates the productive CUS waters from offshore CC waters where levels of primary production are intermediate between those of the upwelling circulation and the oligotrophic NPCG (Figs. 2.2.3, 2.2.5; Collins et al., 2003). CC phytoplankton has variously been suggested to be supported by nutrients (1) advected from the north (Chelton et al., 1982), (2) uplifted from depth via isopycnal tilting (Chelton et al., 1982; Collins et al., 2003), or (3) injected into the CC by the jets, eddies, and fronts that form the western edge of the CUS's coastal upwelling circulation (Barber and Smith, 1981; Collins et al., 2003).

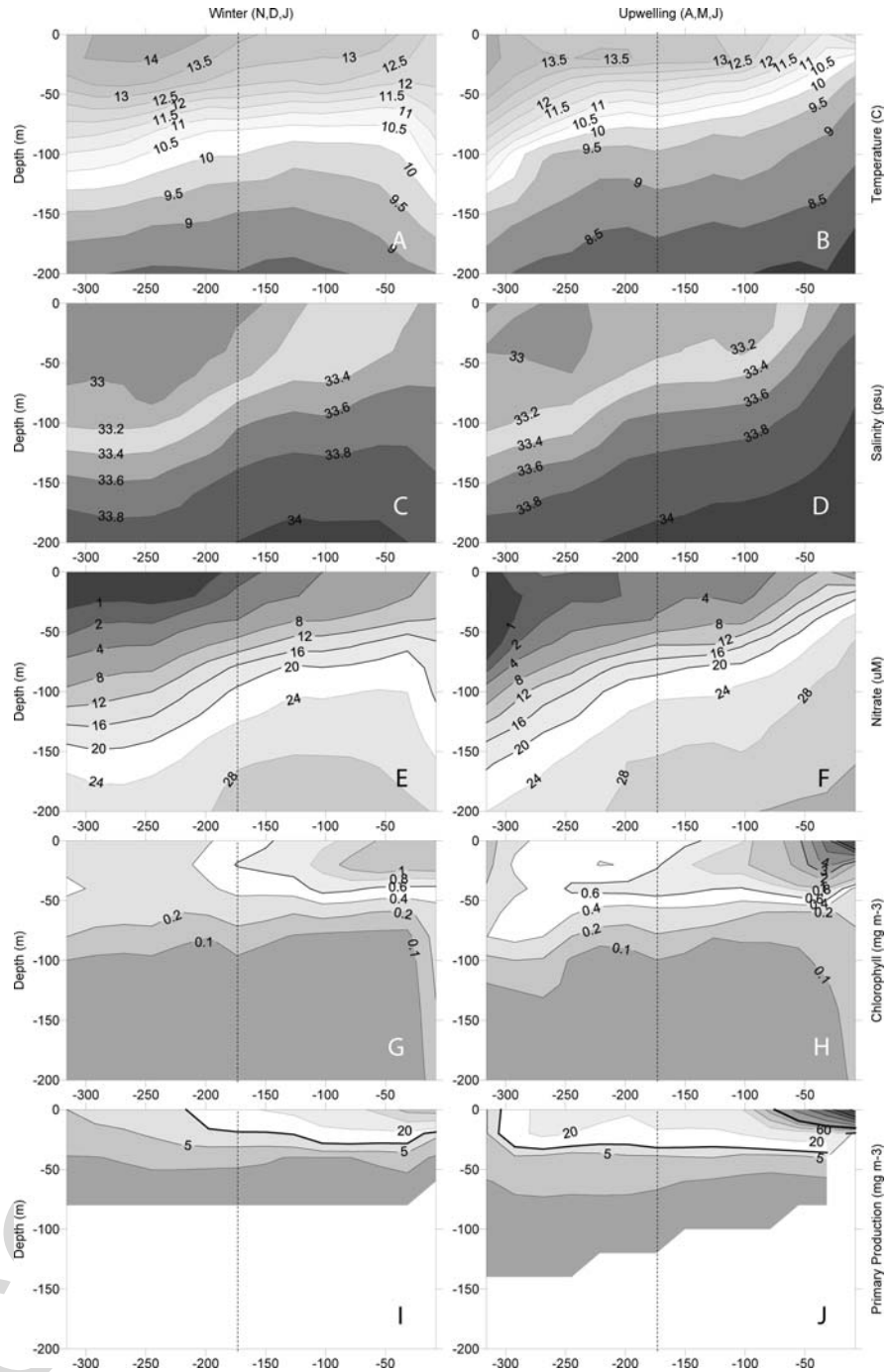

Fig. 2.2.2 Descriptive contours of CC and CUS properties during winter non-upwelling (*left panels*) and spring upwelling months (*right panels*). The *dotted vertical line* indicates average offshore margin of the CUS, at 170 km. The budget was calculated for the CUS only; the CC jet and CC lie offshore of this boundary. Offshore isolines of physical and chemical properties (panels A–F) shoal shoreward in all seasons due to equatorward flow of the CC. Nearshore isolines shallower than about 60 m shoal further in spring due to coastal upwelling. Chlorophyll and primary production values (panels G–J) are highest near the surface inshore due to intersection of the nutricline with the lighted euphotic zone

2.2.1.3 Carbon Budget for the NE Pacific Coastal Transition Zone

Here we assemble a first-estimate carbon budget for the (1) near-surface CUS and (2) flux to the inshore jet or core region of the CC (Fig. 2.2.1). The budget is based on a simple schematic flow diagram (Fig. 2.2.4). The purpose is to initiate a synthesis of carbon flow within this nearshore domain and to highlight processes for which well-founded estimates are lacking.

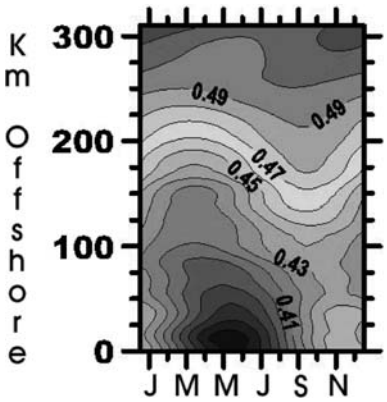

Fig. 2.2.3 Annual cycle of surface layer dynamic height along L67 (from Collins et al., 2003). Dynamic height was calculated for 0/200 m and plotted against distance offshore (*vertical*) and month (*horizontal* axis) based on 9 years of quasi-quarterly cruises 1988–2001. The CC and CUS at top and bottom, respectively, are both in *darker shades*. The CC jet is the horizontal band of tight *light-colored* contours, implying high velocity, that oscillate offshore in winter/spring and onshore in summer/fall; its inshore margin is near the 0.45 dynamic meter contour and is approximately 170 km offshore. This distance has been used in the budget calculations as an offshore boundary for the CUS

We rely heavily on time-series data collected by our laboratory at MBARI in Monterey Bay and along CalCOFI Line 67 off central California (L67; Figs. 2.2.1, 2.2.5). The budget includes estimates for rates of air/sea CO_2 exchange and in-water carbon cycling. The in-water estimates include (1) nitrate imports and exports, (2) particulate organic carbon (POC) exports via diffusion, advection, sinking, conversion to dissolved organic carbon (DOC) and fisheries, and (3) total, new, and recycled primary production.

2.2.2 Budget Components

2.2.2.1 Spatial Domain

The budget estimates surface layer carbon fluxes for the central 750 km of the North American coastal upwelling region between Cape Mendocino and Point Conception in California (40.5–34.4°N; Region A of Fig. 2.2.1), where upwelling dominates the system during spring and summer. L67 lies near the center of this domain.

For L67, Collins et al. (2003) defined the 'CC jet' as a band of strong equatorial surface flow marked by the tightest gradient of dynamic height for the 0–200 m surface layer (Fig. 2.2.3). The jet exhibits a seasonal offshore/onshore oscillation (winter–spring/

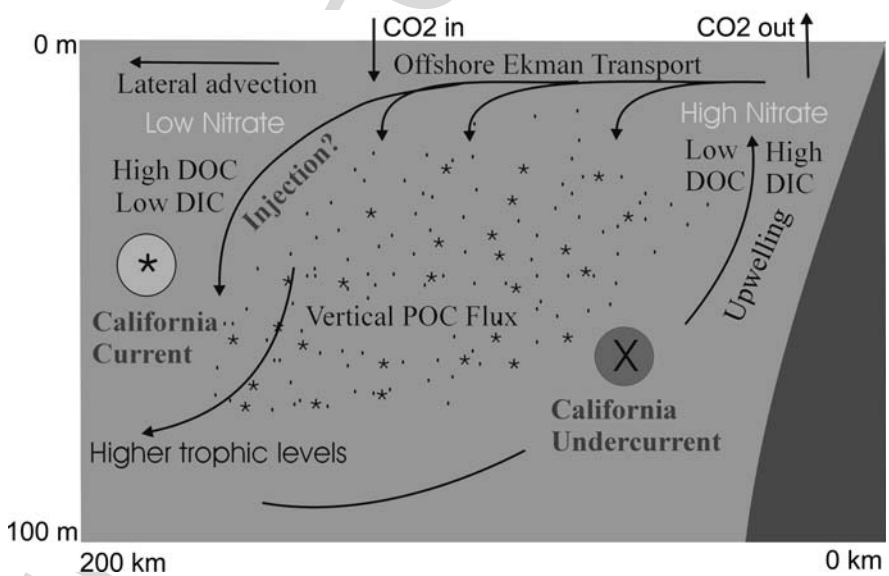

Fig. 2.2.4 Schematic diagram of the CUS and its carbon fluxes. The CC and CUC extend deeper than indicated, and the upwelling indicated includes both geostrophically driven 'pycnocline tilting' (Collins et al., 2003) and wind-driven coastal upwelling. Nitrate and CO_2 are upwelled and partly converted to phytoplankton (POC) via primary production. While moving offshore and southward, the POC sinks, is grazed and converted to dissolved organic carbon (DOC); the remaining nitrate and POC eventually diffuses or advects into or beneath the CC. Estimates for these sources and sinks are presented in Table 2.2.2

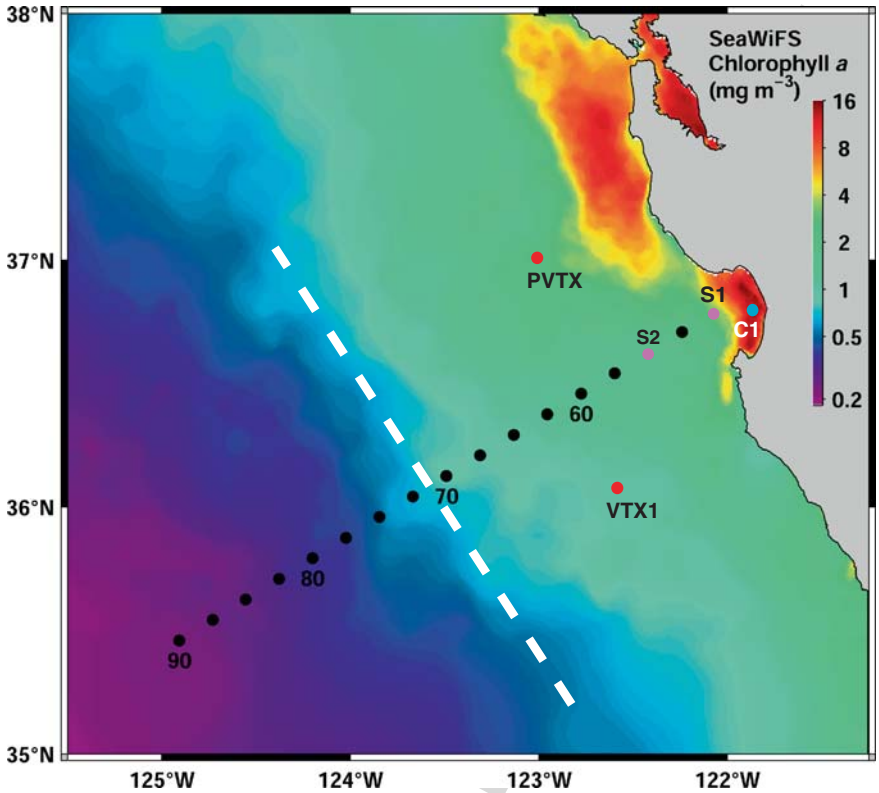

Fig. 2.2.5 Detail composite SeaWIFS surface chlorophyll image showing Monterey Bay (near 36.7° N, 122° W), our Monterey Bay time-series stations occupied each 3 weeks since 1989 (inshore *blue* and *pink circles*), and L67 Stations (*all circles*). Most data used to construct the Table 2.2.2 carbon budget were collected at these stations. Sediment trap data used in the POC flux calculation were obtained at the *pink* (traps S1 and S2) and *red circles* (traps PREVTX and VTX#1 of Martin et al., 1987) and at Station M (not shown, at 34.8° N, 123° W). The M1 mooring/station is not shown but adjacent to the eastern *pink circle*; the M2 mooring/station adjacent to the western *pink circle*. The inshore margin of the CC jet and CC as described in Fig. 2.2.3 and Collins et al. (2003) is shown as *white dashes*, 170 km offshore. The coastal upwelling system or CUS is defined as inshore of the CC jet. The CUS includes stations in three subregions: Monterey Bay, 0–20 km offshore (*blue circle*); an active upwelling region, 20–52 km offshore (*pink circles*); and the coastal transition zone or CTZ, 52–170 km offshore (*black circles* inshore of the *dashed line*)

summer–fall) as well as interannual variations (see Collins et al., 2003), but its inshore margin is near the 0.45 dynamic meter isostere which averages about 170 km offshore (Fig. 2.2.3). This distance has been used as the offshore margin of the CUS for budget calculations.

Ten L67 stations thus lie within the CUS and these fall into three subregions: (1) Monterey Bay, 0–20 km offshore, with one inshore L67 station (blue circle, Fig. 2.2.5); (2) an active upwelling region, one 36° N Rosby Radius wide, 20–52 km offshore, with two L67 stations (pink circles, Fig. 2.2.5; see also Chavez, 1989; Pennington and Chavez, 2000); and (3) a mesoscale mixing region called the Coastal Transition Zone (CTZ; Brink and Cowles, 1991), 52–170 km offshore, with seven L67 stations (black circles inshore of the dashed white line, Fig. 2.2.5). Eight offshore stations on L67, typically within the CC jet, are excluded from the CUS in this analysis (black circles offshore of the dashed line, Fig. 2.2.5).

Budget calculations are restricted to a 0–60 m surface layer, with 60 m being representative of wind-driven Ekman layer depth in mid-latitudes (see Mann and Lazier, 1996). This layer typically includes both the euphotic (lighted) zone and, except in winter, the mixed layer. Upwelling source waters originate from about 60 m (Barber and Smith, 1981; see Fig. 2.2.2A–F).

2.2.2.2 Assumptions

Estimates for the carbon cycle components discussed below are based on the following assumptions which are common to several or all of the estimated fluxes.

1. All units have been expressed as carbon equivalents (g carbon m^{-2} yr^{-1}) using the following bulk conversions as in Chávez et al. (1989):
   - Chlorophyll:nitrogen conversion (1 g chl = 1 mol N)
   - Redfield nitrogen:carbon ratio (1:6.8) and
   - mole:mass carbon conversions (1 mol carbon = 12 g).
2. L67 data are assumed to be representative of the CUS as defined here. This assumption is supported by Chavez et al. (2002) and Fig. 2.2.1 (inset).
3. CUS carbon inputs from north are balanced by losses to the south.

2.2.2.3 Total Production

Total production for the CUS was estimated with on-deck ^{14}C incubations. Productivity profiles were collected at six stations at or inshore of L67 station 70 (Fig. 2.2.5) during 38 'SECRET' cruises (1997–2004) as described by Collins et al. (2003). Details of sample collection, incubation, and analysis are described in Pennington and Chavez (2000). The productivity profiles were depth-integrated over the euphotic zone, averaged within months to weight months equally, then averaged over the year.

2.2.2.4 Upwelling of Nitrate

To estimate nitrate supply, Olivieri and Chavez (2000) used below-thermocline shipboard temperature and nitrate data to derive an empirical relationship for the M1 mooring site (easternmost pink circle, Fig. 2.2.5) which lies in the active upwelling region of L67 – temperature and nitrate are negatively correlated (profiles and equation on Fig. 2.2.6A). We used this

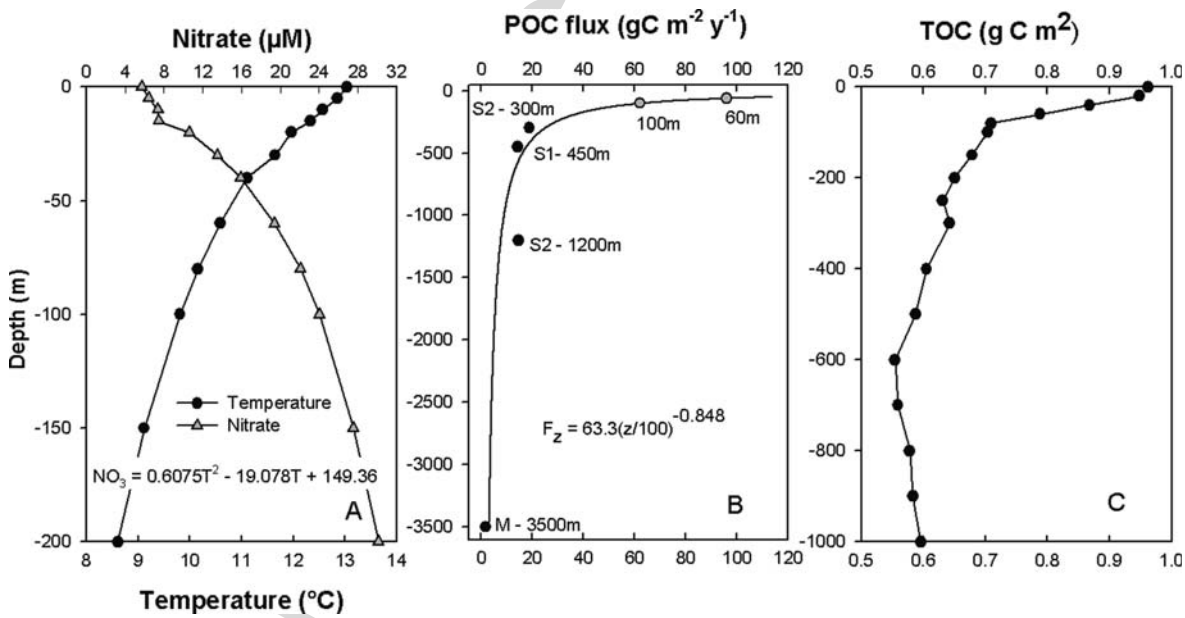

Fig. 2.2.6 (**A**) **Mean temperature and nitrate profiles** based on ship occupations of the M1 mooring site. The nitrate: temperature equation was derived by Olivieri and Chavez (2000) from below-thermocline profile data and used to convert daily 60 m mooring temperatures to the nitrate values used in the calculation of upwelled nitrate. (**B**) **POC flux profile.** *Black circles* are data points as labeled from sediment trap programs cited in the text; the *grey circles* are 60 and 100 m fluxes predicted from the data points with the Martin et al. (1987) power function shown in the figure. Flux values are summarized in Table 2.2.1. **(C) Mean TOC profile** from three CUS stations. TOC has been taken as equivalent to DOC for this winter profile, and the 0–60 m difference as the amount of DOC produced in the euphotic zone per m^3 of water upwelled

relationship to convert 60 m daily average temperatures from the M1 mooring to nitrate values. These nitrate values were then multiplied by daily upwelling volumes per meter of shoreline based on upwelling indices for Monterey Bay (also computed by Olivieri and Chavez, 2000) and the 32,000 m broad upwelling subregion defined above, producing a daily estimate of nitrate flux. This flux was summed over the year and divided by the 170,000 m breadth of the CUS, producing a m^{-2} yr^{-1} estimate for imported or new nitrate, and then converted to carbon equivalents as described above. If the imported nitrate were completely used by CUS phytoplankton, the import could be taken as an estimate of new production. However, it turns out that significant nitrate is exported to the CC by diffusion and advection; these losses are estimated below.

2.2.2.5 Nitrate and POC Exports

Export by Horizontal Diffusion

The rate of diffusive transport of nitrate and particulate organic carbon from the CUS into the CC was estimated as follows. L67 0–60 m mean nitrate and chlorophyll were regressed against distance offshore across the CC jet (96–240 km offshore; Fig. 2.2.7). Values for the active upwelling subregion and the offshore CC were not included because surface layer nitrate and chlorophyll trends are not linear across all of L67 (Fig. 2.2.7); the regression's purpose was to estimate decreases per unit distance offshore across the CUS/CC jet boundary. These negative slopes were converted into carbon equivalents and multiplied by an eddy diffusivity of 10^6 cm^2 s^{-1} (Okubo, 1971), producing diffusive loss estimates dependent on the gradients of 0–60 m nitrate and chlorophyll in the CUS/CC boundary region. Diffusivity is dependent on the scale of interest; the above value was chosen as appropriate for horizontal mixing across the CUS/CC boundary (~100 km; Fig. 2.2.7). Export of nitrate and chlorophyll represents loss of potential and realized new production, respectively.

Export by Advection Offshore

The above calculation pertains to mixing, not advection. Net offshore flow across the CUS/CC jet boundary is driven by Ekman transport and is balanced by onshore flow at depth (see Fig. 2.2.4; reviewed by Mann and Lazier, 1996). If the volume of water upwelled in the active upwelling subregion (Fig. 2.2.5) also approximates the volume-advected offshore across the CUS/CC jet boundary, a simple estimate for the percent of upwelled nitrate exported by advection is (1) the daily upwelling volume times the mean 0–60 m nitrate concentration at the CUS border (3.2 μM NO_3; Fig. 2.2.7A), divided by (2) the daily upwelling volume times the daily 60 m nitrate values at the M1 mooring.

A similar calculation was performed to estimate POC export at the CUS boundary (0.45 mg Chl m^3;

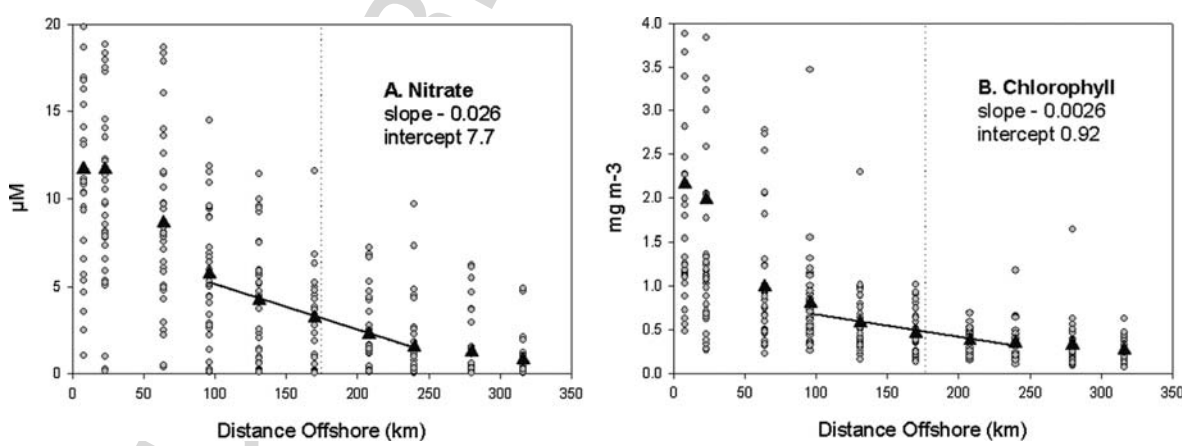

Fig. 2.2.7 Regressions of 0–60 m mean nitrate (A) and chlorophyll (B) against distance offshore across the CUS/CC jet boundary (170 km; *dotted vertical lines*). A few high data points were omitted for clarity. The slopes were multiplied against CUS surface layer diffusivity (Okubo, 1971) to estimate nitrate and POC loss by diffusion. In addition the CUS/CC boundary nitrate (3.2 μM) and chlorophyll (0.45 mg m^{-3}) values were used to estimate upwelling-driven loss due to offshore advection

Fig. 2.2.7B), but with chlorophyll export and nitrate import converted to carbon equivalents (POC).

POC Export by Sinking

POC export by sinking was estimated by averaging 60 m fluxes calculated from six central California carbon flux programs (Table 2.2.1). Martin et al. (1987) deployed sediment traps at two coastal sites, PREVTX and VTX#1 (Fig. 2.2.5, red circles), and produced power functions that estimate coastal POC flux with depth >35 m. We combined the functions for these stations and used the average to estimate 60 and 100 m fluxes from measured fluxes and trap depths (averaged equation on Fig. 2.2.6B). Berelson et al. (1996, 2003) estimated 100 m POC flux off central California, and we extrapolated this flux to 60 m. Pilskaln et al. (1996; Station S1), Chavez (unpublished; Station S2), and Smith et al. (1992; Station M) produced flux data with traps at various depths off central California (S1 and S2 – pink circles, Fig. 2.2.5; Station M – 34.8°N, 123.0°W). POC fluxes at each trap (Fig. 2.2.6B) were again extrapolated to 60 and 100 m. The mean of the extrapolated 60 m fluxes was taken as an estimate of the sinking of POC from the CUS surface layer (Tables 2.2.1 and 2.2.2). Extrapolated 100 m fluxes were included in Table 2.2.1 for comparison with other sediment trap work.

2.2.2.6 POC Conversion to DOC

Dissolved organic carbon (DOC) data are not routinely collected along L67. However, three total organic carbon profiles (TOC; Fig. 2.2.6C) were obtained in the CUS during a February 2003 cruise (stations M1 and M2 – pink circles, Fig. 2.2.5; station UC1 – 36.0°N, 121.8°W). DOC production was estimated on the assumption that the increase in TOC from 60 m to the surface represents the DOC produced in water upwelled into the euphotic zone. POC contribution to TOC was ignored in this winter data. The DOC production estimate was multiplied by the daily upwelling volumes as calculated for new production above and summed to produce an estimate of DOC production $m^{-2}\ yr^{-1}$.

2.2.2.7 Loss to Fisheries

Chavez (1989) estimate that 2–3% of total primary production per year became anchoveta biomass during peak years in the Peruvian upwelling system. If these fish or their feces are recycled in the surface CUS, no flux results. However, if they are removed by fisheries, a carbon export occurs. Lacking fisheries estimates for L67 and the CUS, we use 3% estimate as a placeholder in the current budget.

2.2.2.8 Atmosphere/Ocean CO_2 Exchange

The atmospheric and surface ocean partial pressure of CO_2 (pCO_2) has been measured on over 30 L67 and 140 C1-M2 cruises across the CUS. These and additional atmospheric data (Globalview-CO_2, 2004) were used to estimate the sea surface/air pCO_2 difference (ΔpCO_2) for 1 km binned data for the cruises. A long-term wind and air–sea gas exchange relationship (Wanninkhof, 1992; Wanninkhof and McGillis, 1999)

Table 2.2.1 POC sinking. Fluxes from the trap programs described in the text. Measured fluxes at trap depth were extrapolated to 60 and 100 m with the Martin et al. (1987) power function (Fig. 2.2.6C) averaged for their coastal stations PREVTX and VTX#1 (Fig. 2.2.5). The 100 m fluxes as estimated by Martin et al. (1987) and Berelson et al. (2003) have also been included here; these values were also extrapolated to 60 m. The mean of the 60 m fluxes was entered in the carbon budget, Table 2.2.2. Units are g C $m^{-2}\ yr^{-1}$

Trap	Trap depth (m)	Measured flux	100 m flux	60 m flux	Data source
PVTX, VTX1	50–2000	–	63	98	Martin et al. (1987)
–	100	–	45	69	Berelson et al. (2003)
S2	300	18.8	48	74	Chavez (unpublished)
S1	450	14.4	52	80	Pilskaln et al. (1996)
S2	1200	14.7	121	186	Chavez (unpublished)
M	3500	1.7	34	52	Smith et al. (1992)
Mean (g C $m^{-2}\ yr^{-1}$)			**60**	**93**	

Table 2.2.2 **Annual carbon budget** for the northern and central California coastal upwelling system, with budget estimates expressed as g Carbon m^{-2} yr^{-1}. Nitrate import minus exports is new production, and total production minus new production is recycled production. POC exports are the budgeted portion of new production

	g carbon per m^2	Metric tons carbon per m shore	Metric tons carbon entire CUS	Percent of upwelled nitrate	Percent of new production	Percent of total production
Nitrate flux						
Import – upwelling	204	35	25,995,182	100	121	59
Export – diffusion	2	0.4	301,080	1	1	1
Export – advection	33	6	4,181,244	16	19	10
POC exports						
Diffusion	0.2	0.04	30,108	0.1	0.1	0.1
Advection	5	1	590196	2	3	1
Sinking	93	16	11,857,500	46	55	27
DOC	22	4	2,805,000	11	13	6
Fisheries	10	2	1,317,866	5	6	3
Air/sea CO_2 exchange	0	0	0	0	0	0
Total production	345	59	43,928,850	169	204	100
New production	169	29	21,512,857	83	100	49
Recycled production	176	30	22,415,993	86	104	51
POC exports	130	22	16,600,670	–	77	–
POC+nitrate exports	165	28	21,082,995	81	–	–

was applied to the ΔpCO_2 values and smoothed 30-day winds from the M1 mooring to estimate sea to air flux of carbon. Results from all cruises were combined to derive the mean spatial distribution of the flux. Monthly means can be derived for the C1-M2 region and seasonal means for the L67.

2.2.3 Results and Discussion

Results are presented in Table 2.2.2 and are expressed as g carbon yr^{-1} for each m^{-2} of the CUS, for each m^{-1} of coastline from shore to the CC jet, and for the total CUS as defined above (Region A in Fig. 2.2.1). The fluxes are also expressed as percentages of upwelled nitrate, new, and total production. Nitrate and chlorophyll have been converted to carbon equivalents (POC).

2.2.3.1 Primary Production

Total Production

Total production within the CUS is 345 g carbon m^{-2} yr^{-1} or 4.4×10^7 metric tons of carbon yr^{-1}. CUS total production is overestimated by 39% by a SeaWIFS-based net primary production model (Table 2.2.3; Behrenfeld and Falkowski, 1997) as has been noted previously for L67 (MacFadyen, 1998). Nevertheless, using the model estimates on a per m^2 basis for the boxes in Fig. 2.2.1, CUS total production is nearly threefold higher per m^2 than that in the CC, and fourfold higher m^{-2} than in the NPCG. However, the CUS contributes only ~0.4% of North Pacific primary production and 0.1% to global production. Similarly, the CCS as a whole (Region D of Fig. 2.2.1) contributes 2.9 and 0.7% to North Pacific and global primary production, respectively (Table 2.2.3). In Fig. 2.2.1, regions containing the CUS (A, D) show a pronounced spring/summer SeaWIFS chlorophyll maximum (inset), while offshore CC and NPCG regions (B, C) do not. L67 appears representative of CUS surface chlorophyll (Fig. 2.2.1, inset).

New Production

New production is that supported by 'new' nutrients – typically nitrate – imported into the system and is distinct from 'recycled' production supported by nutrients – typically ammonia – cycled within the euphotic

Table 2.2.3 SeaWIFS-derived total depth-integrated net primary production (TP) for the boxes in Fig. 2.2.1, calculated as in Behrenfeld and Falkowski (1997). 1 gt = 10^{15} g

Zone	Mean TP g C m^{-2} yr^{-1}	Area (m^2)	Zone total g C yr^{-1}	Zone total g t C yr^{-1}	Percent of NPac	Percent of Global
A (CTZ)	481.57	1.71E+11	4.93E+13	0.05	0.4	0.1
B (central CC)	180.34	5.21E+11	9.40E+13	0.09	0.7	0.2
C (NPCG)	122.06	4.92E+11	6.00E+13	0.06		
D (All CC)	212.56	2.06E+12	3.64E+14	0.36	2.9	0.7
NPac total				12.73		
Global				52.22		

zone (Dugdale and Goering, 1967). In the CUS, most new nitrate is supplied to the euphotic zone from below by coastal upwelling (Olivieri and Chavez, 2000). Vertical diffusion and Ekman pumping driven by offshore wind stress curl (see Mann and Lazier, 1996) have not been considered here. If a system's biomass remains constant, then new production is also the fraction of total production available for export, termed the '*f*-ratio' (Dugdale and Goering, 1967). Recycled production is taken as the difference between total and new production.

CUS upwelling of new nitrate can support 204 g carbon m^{-2} yr^{-1} or 59% of the total annual primary productivity along L67 in the CUS (Table 2.2.2). This estimate remains essentially unchanged if one uses a constant 20 μM nitrate input (206 g carbon m^{-2} yr^{-1}) instead of the nitrate:temperature relation employed to produce the estimate in Table 2.2.2. However, it turns out that 17% of the upwelled nitrate is not assimilated by phytoplankton in the CUS, but is apparently exported to the CC by diffusion and advection (equivalent to 35 g carbon m^{-2} yr^{-1}). The remaining 169 g carbon m^{-2} yr^{-1} thus represents our estimate of CUS new production (Table 2.2.2). Chavez and Smith (1995) estimated new production for coastal upwelling regions based on one Sverdrup upwelling per 1000 km coastline and year and 20 μM nitrate source waters. When scaled to our spatial domain, their estimate for new production is almost twice as large as ours (322/169 g carbon m^{-2} yr^{-1}). This substantial difference is due to their higher, and less accurate, estimated upwelling rate (1 vs. the ~0.5 Sv calculated here) and to their assumption of complete utilization of upwelled nitrate.

In spring and summer due to strong equatorward winds, CC and CUS isopycnals shoal (Fig. 2.2.2) as CC velocity and coastal upwelling increase. If new production is calculated based on upwelling season isopycnal tilting rather than on upwelling indices, a much lower estimate is obtained – only 19% of total production (66/345 g carbon m^{-2} yr^{-1}; calculation not shown). Similarly, Collins et al. (2003) calculated that only 20% of Ekman transport is accounted for by isopycnal tilting. Apparently, spring and summer upward displacement of CUS isopycnals is responsible for less than half of the new nitrate brought into the surface layer each year (39% or 66/169 g carbon m^{-2} yr^{-1}). The remainder must be imported by recirculation and along-isopycnal flow.

Our estimate for an *f*-ratio of 0.49 (151/345 g carbon m^{-2} yr^{-1}) is lower than previous estimates for coastal upwelling regions. Chavez and Smith (1995) report a Monterey Bay *f*-ratio of 0.89 with a new production rate of 638 g carbon m^{-2} yr^{-1} for inshore waters during the spring of 1991. The present calculation, however, is reduced by nitrate exports and is for a much larger domain which includes considerable mesotrophic CTZ water offshore of the Monterey Bay observations of Chavez and Smith (1995). Additionally, although we have not produced seasonal estimates, CUS production rates and *f*-ratios are likely higher during the upwelling months than reflected in the annual means of Table 2.2.2. For the Peruvian upwelling system, Dugdale (1985) estimated an *f*-ratio of 0.75 and Chávez et al. (1989) estimated new production at 844 g carbon m^{-2} yr^{-1}, five times greater than our per m^2 estimate for California. This difference is partly procedural. For California the per m^2 rate of new production was effectively reduced by budgeting (1) the broad non-upwelling CTZ as part of the CUS and (2) advective and diffusive nitrate exports. It nevertheless remains true that the active upwelling region of the Peruvian CUS is much broader than that in California due to the increase in Rosby radius at low

latitude (121 vs. 32 km at 9° vs. 36° latitude). Consequently, total CUS nitrate imports and new production are almost certainly several times larger off Peru than California.

2.2.3.2 POC losses

Conversion to DOC

DOC production was estimated as the TOC increase in water upwelled to the surface from 60 m, and accounts for 13 and 6% of CUS new and total production, respectively (Table 2.2.2). This estimate could be increased to 21 and 9% of new and total production if the larger 0–80 m mean TOC difference (32 g carbon m^{-2} yr^{-1}) is used in the calculation, as may be justified by the shape of the profile in Fig. 2.2.7C. In either case the values are based on three wintertime CUS profiles (M1, M2, UC1) – an exceedingly limited data set. We have little concept of DOC cycling or export rates, although one must imagine that like POC, CUS DOC is exported to the CC by both diffusive and advective processes as suggested by Toggweiler and Carson (1995). Our 13% DOC/new production estimate nevertheless compares well with the 10–20% estimates of Hansell and Carlson (1998) and Hansell (2002).

Vertical POC Export by Sinking

Vertical POC export by sinking is substantial and flux through 60 m accounts for 55% of new production. This 93 g carbon m^{-2} yr^{-1} is the mean of extrapolations from six sediment trap programs (Table 2.2.1) using a power function derived from coastal flux measurements (see Methods). This function is data constrained to 35 m (Martin et al., 1987, their Table 2.2.1). Because our budget is for the surface Ekman layer, we extrapolated to a 60 m flux horizon which is shallower than the 100 m (shelf depth) flux typically calculated by sediment trap workers. For comparison with previous work we have included 100 m extrapolated fluxes in Table 2.2.1; these average 60 g carbon m^{-2} yr^{-1} or 36% of new production. The flux reaching 100 m is, as expected, substantially less than that at 60 m, but falls within the wide range of 100 m exports previously estimated for the CUS. Martin et al. (1987) estimated 100 m fluxes of 42 and 85 g carbon m^{-2} yr^{-1} for their coastal stations, Pilskaln et al. (1996) calculated a 100 m flux of 86 g carbon m^{-2} yr^{-1} and Berelson et al. (2003, eqtn. 4) estimated that about 45 g carbon m^{-2} yr^{-1} sinks to the shelf at 100 m. These estimates average 64.5 g carbon m^{-2} yr^{-1}, in agreement with our 100 m value.

If POC sinking flux is normalized to total primary production as 'export-' or '*e*-ratios' and plotted against total production, larger percentages of production are exported by sinking when productivity is low (Fig. 2.2.8). This result is true for the 450 m fluxes reported by Pilskaln et al. (1996) and for the mixed-layer modeled values produced by Olivieri and Chavez (2000). Pilskaln et al. (1996) suggest that when strong upwelling produces high productivity values, rate of advection is also high, minimizing POC flux to sediment traps within the CUS. The 100 m *e*-ratio based on our POC sinking flux from Table 2.2.1 and total production from Table 2.2.2 is 18% – similar to the 19% estimated by Pilskaln et al. (1996; Fig. 2.2.8). Our 60 m *e*-ratio for the base of the Ekman layer is substantially higher at 28%, and Pilskaln et al.'s (1996) 450 m ratio is lower, both as expected. It is not clear, however, why the modeled Olivieri and Chavez (2000) mixed-layer ratios are about half (mean ∼9%) the 100 m values and about one-third the 60 m *e*-ratio (Fig. 2.2.8).

Horizontal Export by Diffusion

Although meandering and often deflected or penetrated by upwelling-associated jets and plumes of the CUS (Figs. 2.2.3; Collins et al., 2003), the CC jet on average flows southeastward, parallel to the coast. CUS carbon is exported horizontally by (1) eddy diffusion and (2) advection of CUS waters into the CC. If upwelling supplies nutrients primarily within the active upwelling subregion (20–52 km of shore), then further offshore all flux terms combined should produce an offshore decline in nutrients (e.g., nitrate) and POC. If the slope of the decline is shallow, diffusive mixing will result in minor net transport across the area for which the slope was determined, which in the present calculation includes the CUS/CC boundary (Fig. 2.2.7). A steep slope implies that diffusion mixes substantial material offshore. Using a CUS diffusivity of 10^6 cm^2 s^{-1}, nitrate and chlorophyll diffusive export accounts for 2 and 0.2% of new production

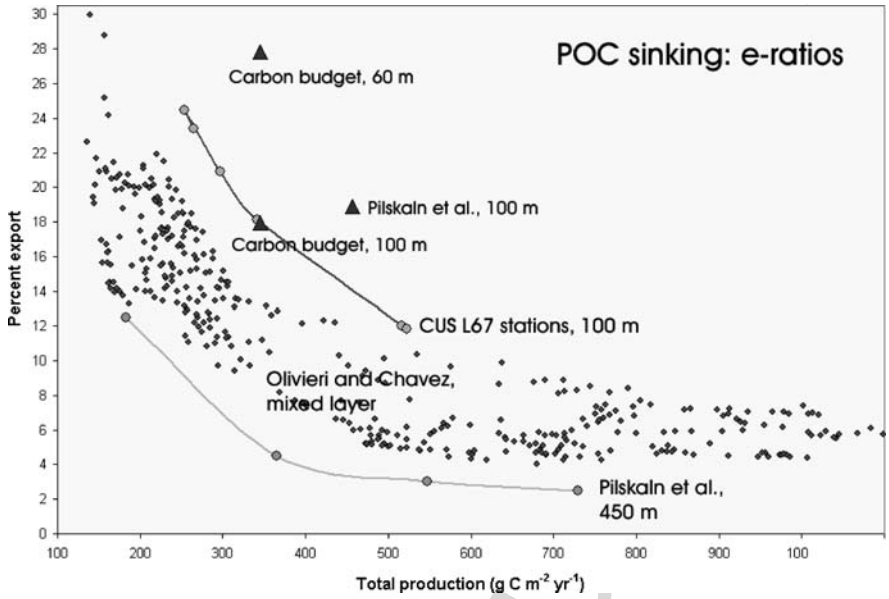

Fig. 2.2.8 Percent export or *e*-ratios (POC flux/total production) plotted against total production, with representative of 450 m data from Pilskaln et al. (1996), mixed-layer model data from Olivieri and Chavez (2000), and CUS L67 data from this paper (100 m extrapolated flux/mean production at individual L67 stations). The *triangles* are mean ratios calculated from Tables 2.2.1 and 2.2.2 and from Pilskaln et al. (1996). The Pilskaln et al. (1996) data and Olivieri and Chavez (2000) model results suggest that higher percentages of production are exported when production is low. The *e*-ratios decrease with depth, as expected, except for the modeled mixed-layer values which are lower than the 100 m extrapolated ratios

(Table 2.2.2), respectively. This diffusivity was chosen as appropriate for a 100 km length scale (see Okubo, 1971), roughly matching the breadth of the CUS or the CUS/CC boundary (Fig. 2.2.7). Our diffusivity is nevertheless almost 100-fold less than the value estimated by Brink et al. (1991) for the CC jet. If the Brink et al. (1991) value is used (8.62×10^7 cm^2 s^{-1}), diffusion is estimated to remove an impossibly large fraction (220/169 g carbon m^{-2} yr^{-1} or 130%) of new production from the CUS. The diffusive export of nitrate represents 1% of that upwelled nearshore (Table 2.2.2).

Export by Advection

During the upwelling season, surface water of the CUS is colder, saltier, and denser than CC surface water (Fig. 2.2.2; reviewed by Pennington and Chavez, 2000; Collins et al., 2003). Net offshore advection of surface CUS waters occurs due to wind-driven Ekman drift and is balanced by onshore flow at depth (see Fig. 2.2.4; reviewed by Mann and Lazier, 1996). Based on the amount of nitrate present in surface waters at the CUS/CC boundary and the rate of offshore flow, we have calculated that, on average, 16% of nitrate upwelled into the surface 60 m is exported across the CUS/CC boundary (Table 2.2.2). In carbon equivalents this export represents 33 g carbon m^{-2} yr^{-1} of potential new production or 19% of new production (Table 2.2.2). A similar calculation based on chlorophyll at the CUS/CC jet boundary suggests that 3% of new production or 5 g carbon m^{-2} yr^{-1} POC may be exported as POC by advection (Table 2.2.2).

Taken together, diffusive and advective export of nitrate across the CUS/CC boundary account for 17% of upwelled nitrate – nitrate apparently not utilized in the CUS and which could increase new production by some 21% (Table 2.2.2). Surface nitrate in the offshore CUS and CC may be underutilized due to iron limitation (Johnson et al., 1999, 2001). If combined with diffusive and advective POC flux, we estimate 20% of CUS potential new production is exported to the CC (40/204 g carbon m^{-2} yr^{-1}). This 20% does not include DOC export to the CC.

Such nutrient and POC advective export may take place at the surface or may occur by subduction at fronts along the CUS/CC jet boundary or inshore. Barth et al. (2002) documented a subduction event

associated with downwelling driven by cyclonic curvature in the flow of a CUS upwelling jet. They estimated that (1) 20% of CUS chlorophyll or 2400 tons of carbon were advected into or beneath the CC during this event and (2) such events occur several times annually. While we note that 246 events of this magnitude would be needed to export 3% of CUS new production – our estimate for advective export of POC – subduction may nevertheless represent an important export process.

Loss to Fisheries

POC is grazed by heterotrophic zooplankton, which in turn are grazed by fish and higher trophic level organisms. Some portion of this POC is excreted by zooplankton as soluble nutrients and is recycled within the euphotic zone – we estimate 51% of CUS total production is supported by such recycled nutrients (176/345 g carbon m^{-2} yr^{-1}; Table 2.2.2). Another portion of grazed POC is defecated – often packaged as fecal pellets – and will be represented in sediment trap estimates of POC sinking. A third portion becomes animal biomass. Some of this biomass is exported by fisheries mortality. Chávez et al. (1989) estimated that 3% of total production is converted into fish biomass (anchoveta) in the coastal upwelling system of Peru. If a similar fraction of total production is converted into fish off northern and central California, then CUS waters could theoretically produce roughly 1,300,000

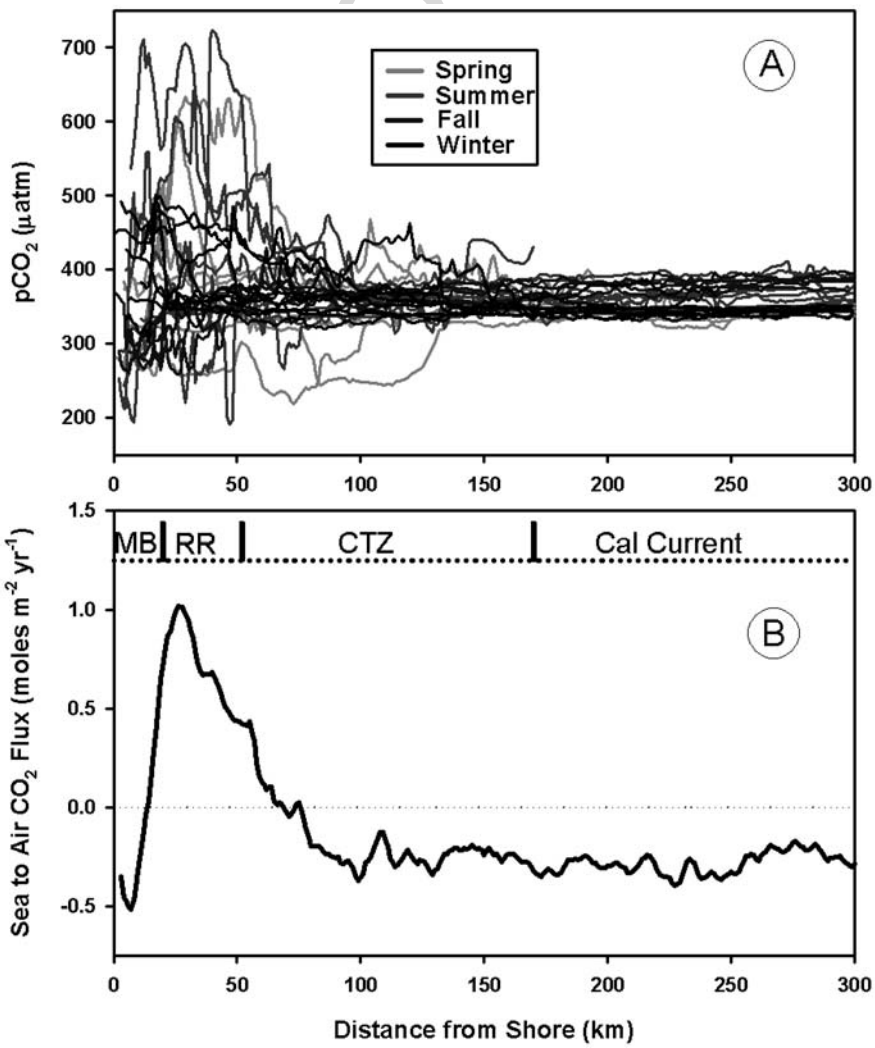

Fig. 2.2.9 Sea surface pCO_2 vs. distance offshore. (A) Variability is high inshore due to intermittent coastal upwelling which is most intense in spring and summer. Offshore variability is due primarily to seasonal temperature differences. (B) Estimate of annual sea to air CO_2 flux based on approximately 150 cruises covering the inner 60 km and 30 cruises covering the remainder of the section. The top of the bottom figure delineates subregions of the section (see Fig. 2.2.5): Monterey Bay (MB), the first Rossby radius region of active upwelling (RR), the coastal transition zone (CTZ), and the CC (offshore of the CUS). Mean annual air/sea CO_2 flux is near-zero within the CUS

metric tons of fish carbon – or 17,000,000 metric tons of fish (carbon to wet weight conversion as in Chavez, 1989) – annually. Lacking estimates of fish or fisheries production in the CUS, we have included the Chavez (1989) 3% in Table 2.2.2 as a placeholder.

2.2.3.3 Atmosphere/Ocean CO_2 Exchange

Measured sea surface pCO_2 values along L67 are high and variable inshore, and lower and less variable in the CC (Fig. 2.2.9A). Within Monterey Bay, shoreward of active upwelling, there is a band between the coast and 20 km offshore that has an average CO_2 flux of about 1 g carbon m^{-2} yr^{-1} CO_2 into the ocean (Fig. 2.2.9B). Within the first Rosby Radius region of active upwelling (20–52 km), CO_2 is on average vented from the ocean on an annual basis (9 g carbon m^{-2} yr^{-1}). The venting occurs primarily in spring and summer; flux reverses and CO_2 diffuses into the ocean in fall (Fig. 2.2.9A). Further offshore in the CUS (52–170 km), CO_2 diffuses into the ocean year round. The net effect of these variations is that, on an annual basis, CUS CO_2 fluxes between the ocean and atmosphere are balanced (Table 2.2.2), with net ocean/atmosphere flux representing less than 0.1% of new production. The physical upwelling of CO_2 nearshore in spring and summer is balanced by biological production and drawdown offshore and in fall and winter.

2.2.4 Conclusion

The carbon budget outlined here is a first attempt to parameterize flow of carbon within the NE Pacific CUS. The partitioning of carbon losses appears fairly reasonable, as the independent estimates for the export components fall within the bounds obtained by others, and when summed, account for 81 and 77% of upwelled nitrate and new production, respectively. The generalization of the L67 budget to the northern and central California CUS provides some idea of regional or system fluxes. An obvious refinement would be the use of latitude-variable upwelling volumes. Except for the pCO2, total and new production estimates along L67, the estimates are at least partly deficient and require more data and better derivation. Our DOC conversion and fisheries estimates are essentially placeholders, awaiting better estimation.

Nevertheless, several conclusions emerge: (1) on an annual basis, CUS air/sea CO_2 flux is near-zero, so that in-water processes dominate carbon flow; (2) sinking represents the largest POC loss term within the CUS, at 55% of new production; and (3) fully 17% of upwelled nitrate is not assimilated by phytoplankton within the CUS. Some portion of CC production is supported by this export, or conversely, this nitrate could increase CUS new production by 21%. The causes and consequences of these results need further exploration.

It is of some interest to consider the budget in relation to climate change. We have presented estimates for mean annual conditions. However, seasonally restricted estimates might be used to gauge the effects of climate change. For example, El Niño enhances and prolongs fall and winter conditions in the CUS (see Chavez et al. 2002). Although we have not prepared such seasonal model budgets, an El Niño (e.g., winter model) budget might be expected to show lower new and total production, lower DOC production, high POC *e*-ratios, less advective export of production to the CC, and a net flux of CO_2 into the ocean (see Chavez et al., 2002). Potential fisheries production should be less. Conversely, La Niña or a cold/anchovy phase of the PDO (see Chavez et al., 2003) (e.g., spring model) could cause increased new and total production, high DOC production, low POC *e*-ratios, more advective export of POC and nitrate to the POC, and perhaps a net flux of CO_2 from the CUS. Fisheries production might increase. CUS width would likely also decrease in the winter model and increase in the spring model (Collins et al., 2003; Chavez et al., 2002), affecting flux totals. Iron supply and the amount of sunlight or fog could also change.

While such predictions can be made for seasonal climate change analogues, it is not clear how global warming – the motivation for this book – might affect the CUS. Bakun (1990) suggested that a warmer earth will result in increased northwesterly wind in the NE Pacific. If so, an enhanced spring model may apply. A spring model may also apply if the subtropics spread poleward, suppressing winter and producing a longer upwelling season in the CUS, as presently occurs in the weakly seasonal, low-latitude Peruvian CUS. Whatever the effects of global warming, it seems likely they will alter carbon cycling by changing the strength or duration of upwelling within the CUS.

The carbon budget and the considerations above are simplistic and highly speculative. We present them as a framework for discussion and encourage others to synthesize their ideas and refine the questions that will be needed to clarify carbon flow processes in NE Pacific and its CUS.

Acknowledgments We thank the David and Lucille Packard Foundation and the U.S. Navy which supported the data collection and analysis reported here. D. Kolber and R. Michisaki prepared the figures.

2.3 The Humboldt Current System[2]

Renato A. Quiñones,
Marcelo H. Gutiérrez, Giovanni Daneri,
Dimitri Gutiérrez Aguilar,
Humberto E. González and
Francisco P. Chavez

The Humboldt Current System (HCS) is one of the most productive marine systems of the world (Fossing et al. 1995, Daneri et al. 2000). Nevertheless, its role in global biogeochemical cycling is still poorly known. The scarcity of data on biogeochemical processes, the strong interannual variability of the HCS and the open nature of its physical borders have severely limited the capacity to generate carbon and nutrient budgets for this region.

The HCS extends, from a latitudinal perspective, from central-south Chile (∼42°S) to northern Peru (∼4–5°S). On its northern limit there is a dynamic boundary with the Pacific Central American Coastal Ecosystem (Bakun et al. 1999) and corresponds to the transition zone between the Humboldt Biogeographic Province and the Panamian Biogeographic Province. This boundary is displaced at seasonal and interannual scales and it is also affected by ENSO phases (Strub et al. 1998).

The southern border of the HCS is related to the West Wind Drift Current (WWDC), which corresponds to the meridional edge of the subtropical gyre which has a permanent anticyclonic circulation in the southern Pacific. In fact the WWDC constitutes the origin of the northward Chile–Peru Current and the southward Cape Horn Current (Reid 1965, Wyrtki 1975, Silva and Neshyba 1977). The WWDC impinges upon the continent from west to northwest direction centred at about 42°S (Nuñez 1996) causing a stagnation point at 44°S around 30 miles from the coast (Dante Figueroa unpublished data). The north–south variability of the bifurcation near the coast results from local wind which, in turn, depends on the interaction between the South Pacific anticyclone and the subpolar lows (Nuñez 1996).

The offshore limit of the HCS is also variable and a matter of discussion. If only the physical domain of upwelling is taken into account the average extension of the ecosystem would be around 120 km off the coast, giving an area of 182 000 km^2, from 4 to 18°S (Chávez and Barber 1987). Nixon and Thomas (2001) used the surface Chl *a* contour line of 1 mg m^{-3} as a criterion to estimate the limit of the ecosystem off the Peruvian coast and found a total area of 220 000 km^2 (140 km width on average) for the 1998/1999 La Niña period, and an area of 120 000 km^2 (80 km width on average) for the 1997/1998 El Niño period. A similar temporal pattern for the whole HCS was observed by Carr (2002), noting a 50% increase of active area in the 1998/1999 annual period with respect to the 1997/1998 annual period for the Peruvian coast. Seasonal change of the extension of productive waters is also observed from maps of surface Chl *a* average distribution (Calienes et al. 1985). Nevertheless, the upwelling influence may extend further offshore. For instance, if a Chl *a* surface concentration of 0.5 mg m^{-3} is used as a threshold level that would give an offshore extension of 250 km or a total area of 400 000 km^2 for the 1998/1999 period (Nixon and Thomas 2000). A rather similar value is obtained if it is followed by the concept of a 'biological width' (Cushing 1971) as 2.5 times the physical width of upwelling (300 km and 450 000 km^2 of width and total area, respectively). AQ6 AQ7

R.A. Quiñones (✉)
Centro de Investigación Oceanográfica en el pacífico Sur oriental (COPAS), Universidad de Concepción, Casilla 160-C, Concepción, Chile; Departamento de Oceanografía, Universidad de Concepción, Casilla 160-C, Concepción, Chile
e-mail: rquinone@udec.cl

[2] We wish to thank Gabriel Yuras for providing SEAWIFS satellite data processing and images. KK Liu and anonymous reviewers provided comments that were very useful to improve this chapter. This chapter was funded by the Centro de Investigación Oceanográfica en el Pacífico Sur oriental (FONDAP-COPAS Grant 150100007; CONICYT, Chile).